# Thermoelectric signature of the nematic phase in hole-doped iron-based superconductors

Marcin Matusiak[*] and Michał Babij

*Institute of Low Temperature and Structure Research, Polish Academy of Sciences, ul. Okolna 2, 50-422 Wroclaw, Poland*

Studies of copper-based superconductors demonstrate how their phase diagram becomes more complex as experimental probes improve, able to distinguish among subtly different electronic phases. One of those phases, nematicity, has become a matter of great interest also in iron-based superconductors, where it is detected deep in the tetragonal state. Here, we present the evolution of in-plane Nernst effect anisotropy in strain-detwinned $Ca(Fe_{1-x}Co_x)_2As_2$ single crystals. We interpret the observed behavior using an approach developed to describe the nematic order parameter in liquid crystals. We also apply the same model to data from other superconductors, $Ba(Fe_{1-x}Co_x)_2As_2$ and $YBa_2Cu_3O_y$. We conclude the observed broken rotational symmetry of the electronic system is a consequence of the emerging thermodynamic electronic nematic order at a temperature much higher than the onset of the magnetic and structural transitions.

## I. INTRODUCTION

The phase diagram of copper-based superconductors, which initially consisted of superconducting and antiferromagnetic phases [1], was subsequently supplemented with regions of occurrence of other electronic orders. These include the pseudogap [2], spin density wave (SDW) [3], as well as three-dimensional (3D) and two-dimensional (2D) charge density wave (CDW) [4,5]. It appears the presence of some kind of electronic nematic order is a pervasive characteristic of unconventional superconductors [6,7], which applies also to iron-based superconductors, where the electronic nematic phase is a distinguished feature of their phase diagram [8]. While there is no agreement yet about a mechanism that leads to the breaking of rotational symmetry in these electron systems, the phenomenon itself has gathered wide experimental support. It was extensively investigated by spectroscopic [9,10] and macroscopic [11,12] probes including studies of the thermoelectrical response anisotropy [13,14]. The latter has turned out to be an invaluable source of information about the nematic phase in cuprates [15,16]. Furthermore, it was argued that this method could detect a type of nematicity that was unreachable by electrical resistivity studies [15].

In this paper, we report measurements of the Nernst effect anisotropy, which indicate the emergence of the nematic phase in electron-doped 122 iron-based superconductors. Notably, the data suggest that at high temperatures we do not observe fluctuations of low-temperature nematic order, but rather a development of a fully set nematicity. Such a possibility was discussed earlier by Tanatar *et al.* [17], and similar conclusions were drawn on the basis of magnetic torque [9] and point contact spectroscopy studies [18]. Very recently, optical measurements indicated that in $Ba(Fe_{1-x}P_x)_2As_2$ the electronic-nematic order emerges in a genuine phase transition [19].

The plausibility of such a scenario was also suggested by another recent study of in-plane thermoelectric anisotropy in a strain-detwinned $Ba(Fe_{1-x}Co_x)_2As_2$ iron-based superconductor [13]. Those results include data on the anisotropy of the Nernst effect ($\Delta\nu$) defined as the difference between the Nernst coefficient determined in the magnetic field parallel to the crystallographic $c$ axis with the thermal gradient imposed either along the $b$ axis ($\nu_b$) or the $a$ axis ($\nu_a$). The striking feature is that $\Delta\nu$ in $Ba(Fe_{1-x}Co_x)_2As_2$ is not affected by the magnetic/structural transition at $T_{tr}$ and $\Delta\nu(T)$ develops smoothly down to the lowest temperatures, changing almost linearly in the semilogarithmic scale. The onset of Nernst anisotropy occurs at a temperature significantly higher than $T_{tr}$, although the fact that the magnetic/structural transition in $Ba(Fe_{1-x}Co_x)_2As_2$ is identified as being second order [20] does not allow one to exclude that nonzero $\Delta\nu$ comes as a result of critical nematic or magnetic fluctuations. The case of $Ca(Fe_{1-x}Co_x)_2As_2$ discussed here is different because the transition in this compound has been classified as being first order (discontinuous) [21,22], thus no substantial contribution from fluctuations is expected.

## II. EXPERIMENT

Single crystals of $Ca(Fe_{1-x}Co_x)_2As_2$ were grown using the Sn-flux method. The Ca, Fe, As, Co, and Sn elements in molar ratios of $1 : (2 - x) : 2 : x : 30$ ($x = 0$, 0.06, and 0.2, respectively, for CaCo0, CaCo3, and CaCo7) were loaded into alumina crucibles and sealed in quartz ampules under vacuum. The ampules were heated slowly to $1050\,°C$, kept at this temperature for several hours, and then cooled down slowly to $650\,°C$ at a rate of $2\,°C/h$. Next, the liquid tin was decanted from the crucibles. The Sn residue on the crystals was removed via etching in diluted hydrochloric acid. The chemical composition of the Co-doped single crystal was determined by an energy-dispersive x-ray analysis.

The Hall coefficient was measured in unstrained crystals in a magnetic field of $B = 12.5\,T$. Then, a sample was mounted

---
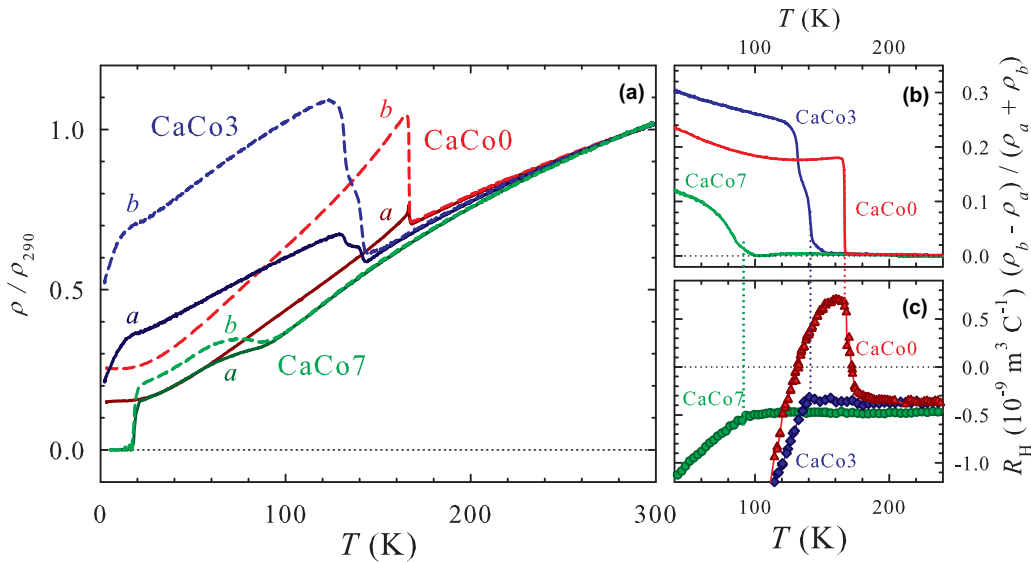
FIG. 1. In-plane electrical transport in the $Ca(Fe_{1-x}Co_x)_2As_2$ series. (a) Temperature dependences of the in-plane electrical resistivity (normalized to the high temperature, $T = 290$ K, value) for detwinned single crystals. There is a clear difference between $\rho$ measured along the long ($a$) and short ($b$) crystallographic axis in the orthorhombic/SDW state. (b) Temperature dependences of the normalized resistivity anisotropy $(\rho_b - \rho_a)/(\rho_a + \rho_b)$ showing no sign of a significant difference between $\rho_a$ and $\rho_b$ high above the structural transition. (c) Anomalies in the temperature dependences of the Hall coefficient occurring at the structural/magnetic transition.

between two clamps made of phosphor bronze and subjected to a uniaxial pressure applied along its sides by a beryllium copper spring controlled with a stepper motor. For the resistivity measurements, the electrical contacts were placed at the corners of a sample and the orientations of the voltage and current leads were switched repetitively during the experiment. This allowed the electrical resistivities $\rho_a$ and $\rho_b$ to be determined using the Montgomery method [23]. The uniaxial pressure was increased step by step and measurements of the resistivity were repeated until a saturation of the anisotropy, indicating maximal detwinning, was achieved. The maximal pressure determined in this way was used during subsequent thermoelectric experiments.

The Nernst coefficient was measured along and across the strain direction in two separate runs with the magnetic field (parallel to the $c$ axis) varied from $-12.5$ to $+12.5$ T. The temperature difference along a sample was determined using two Cernox thermometers as well as a constantan-chromel thermocouple that was calibrated in magnetic field and attached to the sample through few-mm-long and 100-$\mu$m-thick silver wires. Signal leads were made up of long pairs of 25-$\mu$m phosphor bronze wires. $\nu_a$ and $\nu_b$, which differ within several percent due to slightly different geometrical factors in two experimental configurations, are matched by applying a multiplicative correction factor close to 1. More details about the experimental setup are given in Ref. [3].

### III. RESULTS AND DISCUSSION

Figure 1(a) presents electrical resistivity measurements performed along the long ($a$) and short ($b$) crystallographic axes in a series of strain-detwinned $Ca(Fe_{1-x}Co_x)_2As_2$ single crystals with $x = 0$ (CaCo0), 0.03 (CaCo3), and 0.07 (CaCo7). In all samples the transition to the orthorhombic SDW state affects mostly the electrical transport along the

$b$ axis. The anisotropy of the resistivity disappears rather quickly in the tetragonal state as shown in Fig. 1(b), where the normalized temperature dependences of the resistive anisotropy $[\Delta\rho = (\rho_b - \rho_a)/(\rho_b + \rho_a)]$ form a sharp step in CaCo0 at 167 K, a two-step transition in CaCo3 at 148 K (where the structural and magnetic transitions are separated by about 10 K), and a rather smooth development of $\Delta\rho$ below 100 K in CaCo7. The Hall coefficient, whose temperature dependences in the vicinity of the transitions are presented in Fig. 1(c), exhibits an anomaly at the respective temperatures in all three samples, which is not exactly the case for the Nernst coefficient presented in Fig. 2(a). While $\nu(T)$ in CaCo0 and CaCo3 exhibit a clear steplike change at the structural/magnetic transition (which might be related to the presence of Dirac fermions in the SDW phase of the 122 iron-based superconductors [24,25]), such an anomaly is absent in CaCo7. Figure 2(b), presenting the temperature and doping evolution of the Nernst anisotropy calculated as $\Delta\nu = \nu_a - \nu_b$, indicates that $\Delta\nu$ in CaCo0 and CaCo3 changes sign below $T_{tr}$, whereas for all three samples $\Delta\nu$ is positive in the tetragonal state. This is different from $Ba(Fe_{1-x}Co_x)_2As_2$, where $(\nu_a - \nu_b)$ is negative for all samples being studied except for the most doped $Ba(Fe_{0.94}Co_{0.06})_2As_2$, where $\Delta\nu$ is small but positive. Interestingly, the onset of $\Delta\nu$ shown in Fig. 2(c) occurs at temperatures significantly higher than each respective $T_{tr}$. Namely, they are $T^* \approx 275$, 280, and 250 K for CaCo0, CaCo3, and CaCo7, respectively. Remarkably, these values, placed on the $x$-$T$ phase diagram shown in Fig. 3, closely correspond to the analogous temperatures determined for the $Ba(Fe_{1-x}Co_x)_2As_2$ series [13]. The phase diagrams for both compounds are normalized to match the range of existence of the SDW phase, i.e., $T$ values are divided by the $T_{SDW}$ for respective parent compounds ($BaFe_2As_2$ or $CaFe_2As_2$), whereas $x$ values are divided by the respective $x_{SDW}$ that is
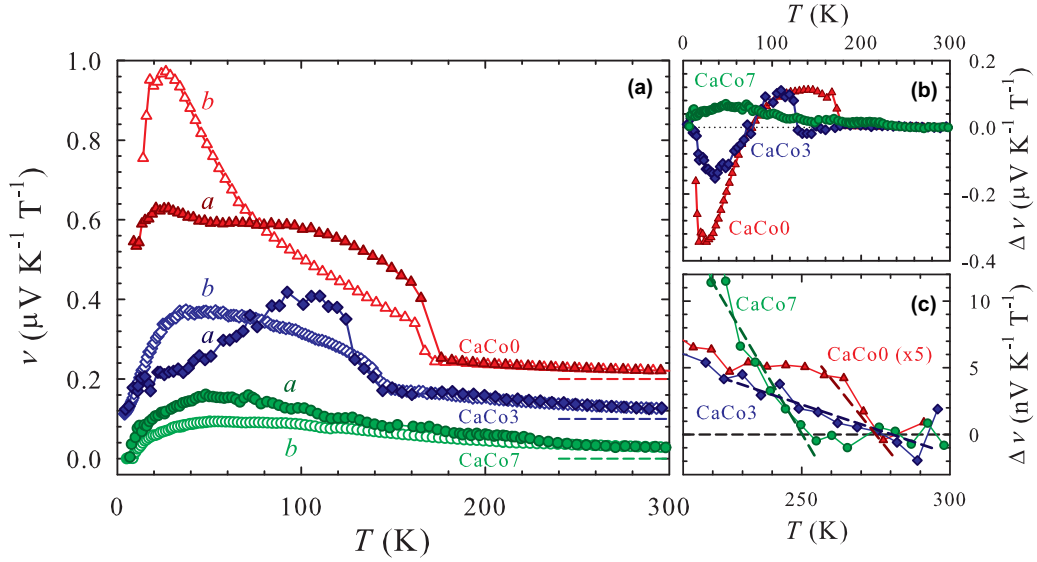
FIG. 2. In-plane magnetothermoelectric response in the $Ca(Fe_{1-x}Co_x)_2As_2$ series. (a) Temperature dependences of the Nernst coefficient for the heat current being imposed along either the $a$ or $b$ orthorhombic axis. CaCo3 and CaCo0 plots are shifted vertically by $1 \times 10^{-10}$ and $2 \times 10^{-10}$ V K$^{-1}$ T$^{-1}$, respectively, for the sake of clarity, with dashed lines denoting the corresponding $\nu = 0$ V K$^{-1}$ T$^{-1}$ levels. (b) Temperature dependence of the Nernst coefficient anisotropy defined as $\Delta\nu = \nu_a - \nu_b$. (c) High-temperature onset of the Nernst anisotropy.

the cobalt content at which SDW disappears in the $T = 0$ K limit.

Perhaps the most important outcome of this work is the set of temperature dependences of the Nernst anisotropy shown in Fig. 4(a). We notice that $\Delta\nu$ for $Ca(Fe_{1-x}Co_x)_2As_2$ has an opposite sign to $\Delta\nu$ for $Ba(Fe_{1-x}Co_x)_2As_2$ (except for BaCo6) but it is not trivial to explain. The normal-state Nernst coefficient is composed of two terms: $\nu = (\frac{\alpha_{xy}}{\sigma} - S\tan\theta)\frac{1}{B}$ (where $\alpha_{xy}$ is the off-diagonal element of the Peltier ten-



FIG. 3. Schematic $x$-$T$ phase diagram of $Ca(Fe_{1-x}Co_x)_2As_2$ [35] and $Ba(Fe_{1-x}Co_x)_2As_2$ [36] with marked positions of the onset of the Nernst anisotropy. Results for $Ca(Fe_{1-x}Co_x)_2As_2$ are marked with solid red points and for $Ba(Fe_{1-x}Co_x)_2As_2$ with open red points. Yellow and dark yellow regions in the phase diagram denote the spin density wave phase; pink and dark pink—orthorhombic, nonmagnetic phase; blue and dark blue—superconducting phase.

sor, and $\theta$ is the Hall angle) and its sign depends on details of the electronic structure and scattering processes. The explanation of the sign change of the $(\nu_a - \nu_b)$ difference between $Ca(Fe_{1-x}Co_x)_2As_2$ and $Ba(Fe_{1-x}Co_x)_2As_2$, which is unlikely incidental, would require a much more elaborate approach than the one offered in the present work. Therefore, in Fig. 4(a), we plot the absolute value of the Nernst anisotropy divided by $T$ to account for the fact that the Nernst coefficient, being a measure of transverse entropy flow [26], inevitably decreases with decreasing temperature. At the structural/magnetic transition $|\Delta\nu|/T$ changes abruptly in CaCo0 and CaCo3, perhaps due to a potent contribution to the Nernst coefficient from the aforementioned Dirac fermions or as a signature of the strong first-order character of the transition [8]. In contrast, $|\Delta\nu|/T$ in CaCo7 seems to be unaffected by the formation of the orthorhombic/SDW state. Notably, the character of the $|\Delta\nu|/T$ temperature dependence is shared among all the samples studied, and the behavior of $|\Delta\nu|/T(T)$ is far from the $\frac{C}{T-T_c}$ form expected for the Curie-Weiss behavior. The latter was suggested to be caused (with some deviations) by critical fluctuations of the nematic state in iron-based superconductors studied by means of elastoresistance measurements [12]. As a matter of fact, our data are much better fitted by the equation proposed by Haller to describe the behavior of the nematic order parameter $Q$ in liquid crystals [27], $Q = (1 - \frac{T}{T^*})^\beta$, where $T^*$ is a characteristic temperature somewhat lower than the actual temperature of the discontinuous nematic-isotropic transition. The actual fits, $\frac{|\Delta\nu|}{T} = \alpha(1 - \frac{T}{T^*})^\beta$, have only two free parameters ($\alpha$ and $\beta$) since $T^*$ values are taken as the temperatures of the onset of Nernst anisotropy [Fig. 2(c)]. Here, $\alpha$ is the proportional constant and $\beta$ is the pseudocritical exponent. Some deviations from the fitting curves near $T^*$ could be a result of the empirical nature of the Haller's approximation equation, which is not expected to be accurate close to the transition temperature [28].
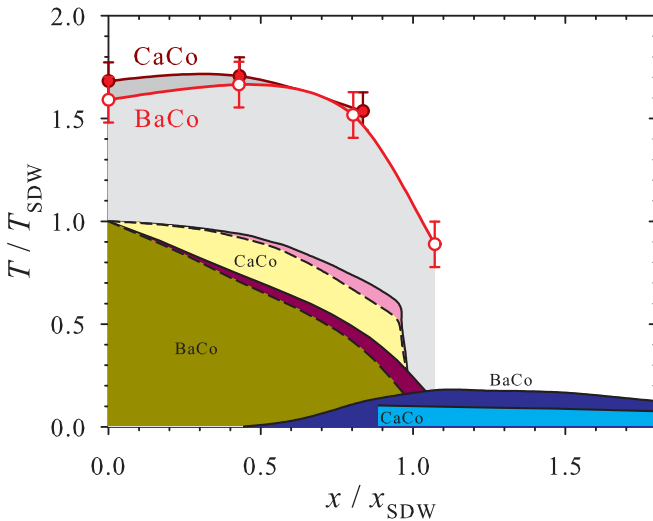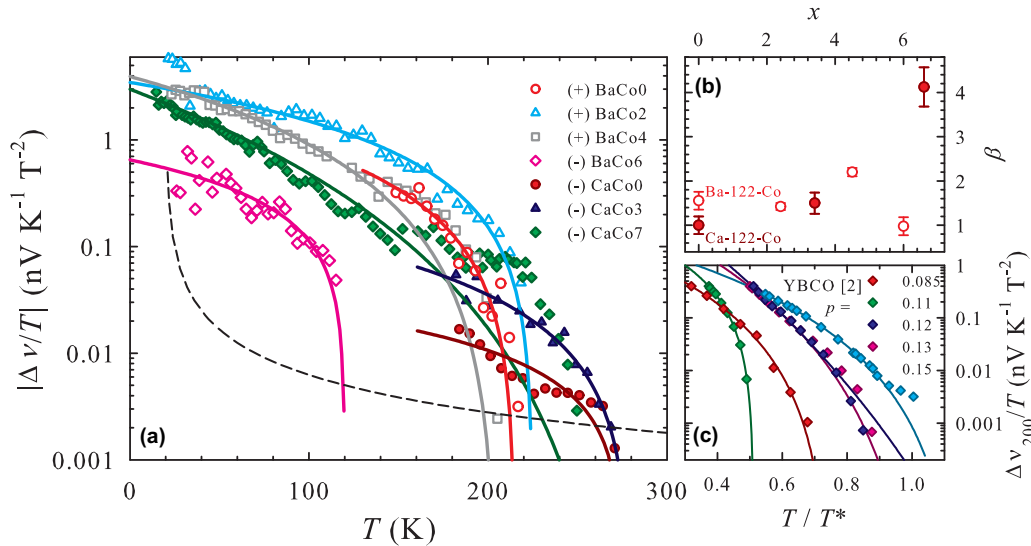
FIG. 4. Anisotropy of the Nernst coefficient as a measure of the electronic nematic order parameter in iron- and copper-based super-conductors. (a) Temperature dependences of the absolute value of $\Delta\nu/T$ for the $Ca(Fe_{1-x}Co_x)_2As_2$ (solid symbols) and $Ba(Fe_{1-x}Co_x)_2As_2$ [13] (open symbols) series, where "(+)" and "(−)" marks denote the positive and negative sign of $\Delta\nu/T$, respectively. Solid lines are fits to the temperature dependence of the nematic order parameters considered in liquid crystals [27], whereas the dashed line is an exemplary Curie-Weiss-type dependence $\Delta\nu/T = \frac{5\times10^{-10}}{T-20}$. (b) Changes of the $\beta$ parameter with doping that are supposedly reflecting the increasing level of disorder. (c) Nernst anisotropy in $YBa_2Cu_3O_y$, where $\Delta\nu_{200} = \Delta\nu(T) - \Delta\nu(200\,\text{K})$ and the temperature axis is also normalized [15]. Solid lines give fits for the nematic order parameter as mentioned in the text.

The pseudocritical exponent $\beta$ shown in Fig. 4(b) stays within the 1–4 range for $(Ca, Ba)(Fe_{1-x}Co_x)_2As_2$, which is about one order of magnitude higher than values observed in liquid crystals [27,28]. According to Ranjkesh *et al.*, the pseudocritical exponent is supposed to rise with the concentrations of impurities [28], and the estimated $\beta$ in $(Ba, Co)(Fe_{1-x}Co_x)_2As_2$ seems to roughly obey this rule increasing with $x$ (since the growing substitution of iron with cobalt inevitably leads to an increased disorder), although the data scattering does not allow us to draw a definitive conclusion.

Here, we would like to note that the data from an analogous experiment performed on $YBa_2Cu_3O_y$ [15], presented in Fig. 4(c), can also be very well fitted with the Haller equation (this time $T^*$ is taken as a free parameter). Such a universal behavior of the $|\Delta\nu|/T$ temperature dependence, along with the fact that $|\Delta\nu|/T$ is unaffected by the structural/magnetic transition in CaCo7 as well as in $Ba(Fe_{1-x}Co_x)_2As_2$ with $x = 0.02$ and $0.04$ [13], suggests the anisotropy of the Nernst coefficient might be a proxy of the electronic-nematic order parameter. This idea was already considered by Daou *et al.* [16], who were inspired by an analogous proposition by Borzi *et al.* [29] to define the phenomenological nematic order parameter in $Sr_3Ru_2O_7$ as the in-plane anisotropy of the electrical resistivity. A remaining question is why we observe broken rotational symmetry in the thermoelectrical studies, which is inaccessible to electrical measurements and vice versa—that is, why is the anomaly at the transition that is clearly visible in $\Delta\rho(T)$, absent in $\Delta\nu(T)$? While we cannot provide a firm answer, there are possible scenarios that could explain such intriguing behavior. First, there are well-known examples of electronic systems with decoupled charge and entropy fluxes. One of them is the superconducting

state where Cooper pairs conduct charge without dissipation but do not contribute in entropy transport. Others are small-angle electron-phonon scattering processes, which effectively disturb entropy transport with only little effect on the charge transfer. Remarkably, the latter play an important role in strongly correlated electron systems, where charge transport could be described as the flow of a hydrodynamic electron fluid [30]. In such a case the energy dissipation is dominated by momentum-conserving small-angle electron-phonon scattering [31]. Therefore, if charge carriers in the electronic-nematic state suffer from anisotropic, but small-angle, scattering, it will be seen in the anisotropy of the Nernst effect, but will be insignificant for electrical resistivity measurements. A similar phenomenon was recently observed in $YBa_2Cu_3O_y$ and attributed to the emergence of short-range charge density wave modulations [15]. On the other hand, a possible reason why the anomaly at the magnetic/structural transition is absent in the $|\Delta\nu|/T$ temperature dependence was proposed in Ref. [3]. Namely, large-angle elastic scattering might cancel out for Nernst anisotropy which consists of contributions from both $a$- and $b$-direction transport. In fact, $\Delta\nu$ can be expressed as a subtraction of a two Sondheimer cancellations [32], one for the $a$ direction, another one for the $b$ direction [13], and in metals the resulting difference might be insignificant.

## IV. CONCLUSION

In summary, we show that in the phase diagram of iron-based superconductors, in a way similar to their copper-based counterparts, there is room for another electronically driven ordered state. Using Nernst anisotropy as a proxy of the electronic-nematic order parameter, we indicate the emergence of a high-temperature true nematic phase. Even

though we are not able to pinpoint its possible origin [8], we stress the role of the elastic and inelastic scattering in the process. The electronic-nematic phase arises at high temperature and can develop smoothly despite the occurrence of a magnetic/structural transition. The present form of the phase diagram does not exclude that the electronic-nematic phase ceases when the superconducting critical temperature reaches its maximum, which would once again be common behavior for iron-based and copper-based supercoductors [33]. Perhaps it might even suggest an intimate relation between the electronic nematicity and superconductivity [34].

[1] A. W. Sleight, Chemistry of high-temperature superconductors, Science **242**, 1519 (1988).

[2] H. Ding, T. Yokoya, J. C. Campuzano, T. Takahashi, M. Randeria, M. R. Norman, T. Mochiku, K. Kadowaki, and J. Giapintzakis, Spectroscopic evidence for a pseudogap in the normal state of underdoped high-$T_c$ superconductors, Nature (London) **382**, 51 (1996).

[3] D. Haug, V. Hinkov, Y. Sidis, P. Bourges, N. B. Christensen, A. Ivanov, T. Keller, C. T. Lin, and B. Keimer, Neutron scattering study of the magnetic phase diagram of underdoped YBa$_2$Cu$_3$O$_{6+x}$, New J. Phys. **12**, 105006 (2010).

[4] T. Wu, H. Mayaffre, S. Krämer, M. Horvatić, C. Berthier, W. N. Hardy, R. Liang, D. A. Bonn, and M.-H. Julien, Magnetic-field-induced charge-stripe order in the high-temperature superconductor YBa$_2$Cu$_3$O$_y$, Nature (London) **477**, 191 (2011).

[5] F. Laliberté, M. Frachet, S. Benhabib, B. Borgnic, T. Loew, J. Porras, M. Le Tacon, B. Keimer, S. Wiedmann, C. Proust, and D. LeBoeuf, High field charge order across the phase diagram of YBa$_2$Cu$_3$O$_y$, npj Quantum Mater. **3**, 11 (2018).

[6] E. Fradkin, S. A. Kivelson, M. J. Lawler, J. P. Eisenstein, and A. P. Mackenzie, Nematic Fermi fluids in condensed matter physics, Annu. Rev. Condens. Matter Phys. **1**, 153 (2010).

[7] J. Wu, A. T. Bollinger, X. He, and I. Božović, Pervasive electronic nematicity in a cuprate superconductor, Physica C **549**, 95 (2018).

[8] R. M. Fernandes, A. V. Chubukov, and J. Schmalian, What drives nematic order in iron-based superconductors? Nat. Phys. **10**, 97 (2014).

[9] S. Kasahara, H. J. Shi, K. Hashimoto, S. Tonegawa, Y. Mizukami, T. Shibauchi, K. Sugimoto, T. Fukuda, T. Terashima, A. H. Nevidomskyy, and Y. Matsuda, Electronic nematicity above the structural and superconducting transition in BaFe$_2$(As$_{1-x}$P$_x$)$_2$, Nature (London) **486**, 382 (2012).

[10] S. Avci, O. Chmaissem, J. M. Allred, S. Rosenkranz, I. Eremin, A. V. Chubukov, D. E. Bugaris, D. Y. Chung, M. G. Kanatzidis, J.-P. Castellan, J. A. Schlueter, H. Claus, D. D. Khalyavin, P. Manuel, A. Daoud-Aladine, and R. Osborn, Magnetically driven suppression of nematic order in an iron-based superconductor, Nat. Commun. **5**, 3845 (2014).

[11] E. C. Blomberg, M. A. Tanatar, R. M. Fernandes, I. I. Mazin, B. Shen, H.-H. Wen, M. D. Johannes, J. Schmalian, and R. Prozorov, Sign-reversal of the in-plane resistivity anisotropy in hole-doped iron pnictides, Nat. Commun. **4**, 1914 (2013).

[12] H.-H. Kuo, J.-H. Chu, J. C. Palmstrom, S. A. Kivelson, and I. R. Fisher, Ubiquitous signatures of nematic quantum criticality in optimally doped Fe-based superconductors, Science **352**, 958 (2016).

[13] M. Matusiak, K. Rogacki, and T. Wolf, Thermoelectric anisotropy in the iron-based superconductor Ba(Fe$_{1-x}$Co$_x$)$_2$As$_2$, Phys. Rev. B **97**, 220501(R) (2018).

[14] M. Matusiak, M. Babij, and T. Wolf, Anisotropy of the Seebeck and Nernst coefficients in parent compounds of the iron-based superconductors, Phys. Rev. B **97**, 100506(R) (2018).

[15] O. Cyr-Choinière, G. Grissonnanche, S. Badoux, J. Day, D. A. Bonn, W. N. Hardy, R. Liang, N. Doiron-Leyraud, and L. Taillefer, Two types of nematicity in the phase diagram of the cuprate superconductor YBa$_2$Cu$_3$O$_y$, Phys. Rev. B **92**, 224502 (2015).

[16] R. Daou, J. Chang, D. LeBoeuf, O. Cyr-Choinière, F. Laliberté, N. Doiron-Leyraud, B. J. Ramshaw, R. Liang, D. A. Bonn, W. N. Hardy, and L. Taillefer, Broken rotational symmetry in the pseudogap phase of a high-$T_c$ superconductor, Nature (London) **463**, 519 (2010).

[17] M. A. Tanatar, E. C. Blomberg, A. Kreyssig, M. G. Kim, N. Ni, A. Thaler, S. L. Bud'ko, P. C. Canfield, A. I. Goldman, I. I. Mazin, and R. Prozorov, Uniaxial-strain mechanical detwinning of CaFe$_2$As$_2$ and BaFe$_2$As$_2$ crystals: Optical and transport study, Phys. Rev. B **81**, 184508 (2010).

[18] H. Z. Arham, C. R. Hunt, W. K. Park, J. Gillett, S. D. Das, S. E. Sebastian, Z. J. Xu, J. S. Wen, Z. W. Lin, Q. Li, G. Gu, A. Thaler, S. L. Budko, P. C. Canfield, and L. H. Greene, Gap-like feature in the normal state of $X$(Fe$_{1-x}$Co$_x$)$_2$As$_2$, $X$ = Ba, Sr and Fe$_{1+y}$ Te revealed by point contact spectroscopy, J. Phys.: Conf. Ser. **400**, 022001 (2012).

[19] E. Thewalt, I. M. Hayes, J. P. Hinton, A. Little, S. Patankar, L. Wu, T. Helm, C. V. Stan, N. Tamura, J. G. Analytis, and J. Orenstein, Imaging Anomalous Nematic Order and Strain in Optimally Doped BaFe(As, P)$_2$, Phys. Rev. Lett. **121**, 027001 (2018).

[20] D. K. Pratt, W. Tian, A. Kreyssig, J. L. Zarestky, S. Nandi, N. Ni, S. L. Bud'ko, P. C. Canfield, A. I. Goldman, and R. J. McQueeney, Coexistence of Competing Antiferromagnetic and Superconducting Phases in the Underdoped Ba(Fe$_{0.953}$Co$_{0.047}$)$_2$As$_2$ Compound Using X-ray and Neutron Scattering Techniques, Phys. Rev. Lett. **103**, 087001 (2009).

[21] S. L. Bud'ko, S. Ran, and P. C. Canfield, Thermal expansion of CaFe$_2$As$_2$: Effect of cobalt doping and postgrowth thermal treatment, Phys. Rev. B **88**, 064513 (2013).

[22] A. Fente, A. Correa-Orellana, A. E. Böhmer, A. Kreyssig, S. Ran, S. L. Bud'ko, P. C. Canfield, F. J. Mompean, M. García-Hernández, C. Munuera, I. Guillamón, and H. Suderow, Direct visualization of phase separation between superconducting and nematic domains in Co-doped CaFe$_2$As$_2$ close to a first-order phase transition, Phys. Rev. B **97**, 014505 (2018).

[23] H. C. Montgomery, Method for measuring electrical resistivity of anisotropic materials, J. Appl. Phys. **42**, 2971 (1971).

[24] T. Morinari, E. Kaneshita, and T. Tohyama, Topological and Transport Properties of Dirac Fermions in an Antiferromagnetic Metallic Phase of Iron-Based Superconductors, Phys. Rev. Lett. **105**, 037203 (2010).

[25] Z.-G. Chen, L. Wang, Y. Song, X. Lu, H. Luo, C. Zhang, P. Dai, Z. Yin, K. Haule, and G. Kotliar, Two-Dimensional Massless Dirac Fermions in Antiferromagnetic $A\mathrm{Fe_2As_2}$ ($A$ = Ba, Sr), Phys. Rev. Lett. **119**, 096401 (2017).

[26] K. Behnia and H. Aubin, Nernst effect in metals and superconductors: A review of concepts and experiments, Rep. Prog. Phys. **79**, 046502 (2016).

[27] I. Haller, Thermodynamic and static properties of liquid crystals, Solid State Chem. **10**, 103 (1975).

[28] A. Ranjkesh, M. Cvetko, J.-C. Choi, and H.-R. Kim, Phase and structural order in mixture of nematic liquid crystals and anisotropic nanoparticles, Phase Transitions **90**, 423 (2017).

[29] R. A. Borzi, S. A. Grigera, J. Farrell, R. S. Perry, S. J. S. Lister, S. L. Lee, D. A. Tennant, Y. Maeno, and A. P. Mackenzie, Formation of a nematic fluid at high fields in $\mathrm{Sr_3Ru_2O_7}$, Science **315**, 214 (2007).

[30] J. Gooth, F. Menges, N. Kumar, V. Süß, C. Shekhar, Y. Sun, U. Drechsler, R. Zierold, C. Felser, and B. Gotsmann, Thermal and electrical signatures of a hydrodynamic electron fluid in tungsten diphosphide, Nat. Commun. **9**, 4093 (2018).

[31] R. N. Gurzhi, Hydrodynamic effects in solids at low temperature, Sov. Phys. Usp. **11**, 255 (1968).

[32] E. H. Sondheimer, The theory of the galvanomagnetic and thermomagnetic effects in metals, Proc. R. Soc. London, Ser. A **193**, 484 (1948).

[33] C. Proust and L. Taillefer, The remarkable underlying ground states of cuprate superconductors, Annu. Rev. Condens. Matter Phys. **10**, 409 (2019).

[34] S. Lederer, Y. Schattner, E. Berg, and S. A. Kivelson, Enhancement of Superconductivity near a Nematic Quantum Critical Point, Phys. Rev. Lett. **114**, 097001 (2015).

[35] L. Harnagea, S. Singh, G. Friemel, N. Leps, D. Bombor, M. Abdel-Hafiez, A. U. B. Wolter, C. Hess, R. Klingeler, G. Behr, S. Wurmehl, and B. Büchner, Phase diagram of the iron arsenide superconductors $\mathrm{Ca(Fe_{1-x}Co_x)_2As_2}$ ($0 \leqslant x \leqslant 0.2$), Phys. Rev. B **83**, 094523 (2011).

[36] J.-H. Chu, J. G. Analytis, C. Kucharczyk, and I. R. Fisher, Determination of the phase diagram of the electron-doped superconductor $\mathrm{Ba(Fe_{1-x}Co_x)_2As_2}$, Phys. Rev. B **79**, 014506 (2009).